Reconstruction of ensembles of nonlinear neurooscillators with sigmoid coupling function

Ilya V. Sysoev, Vladimir I. Ponomarenko & Mikhail D. Prokhorov

Nonlinear Dynamics
An International Journal of Nonlinear Dynamics and Chaos in Engineering Systems

ISSN 0924-090X
Volume 95
Number 3

Nonlinear Dyn (2019) 95:2103-2116
DOI 10.1007/s11071-018-4679-y

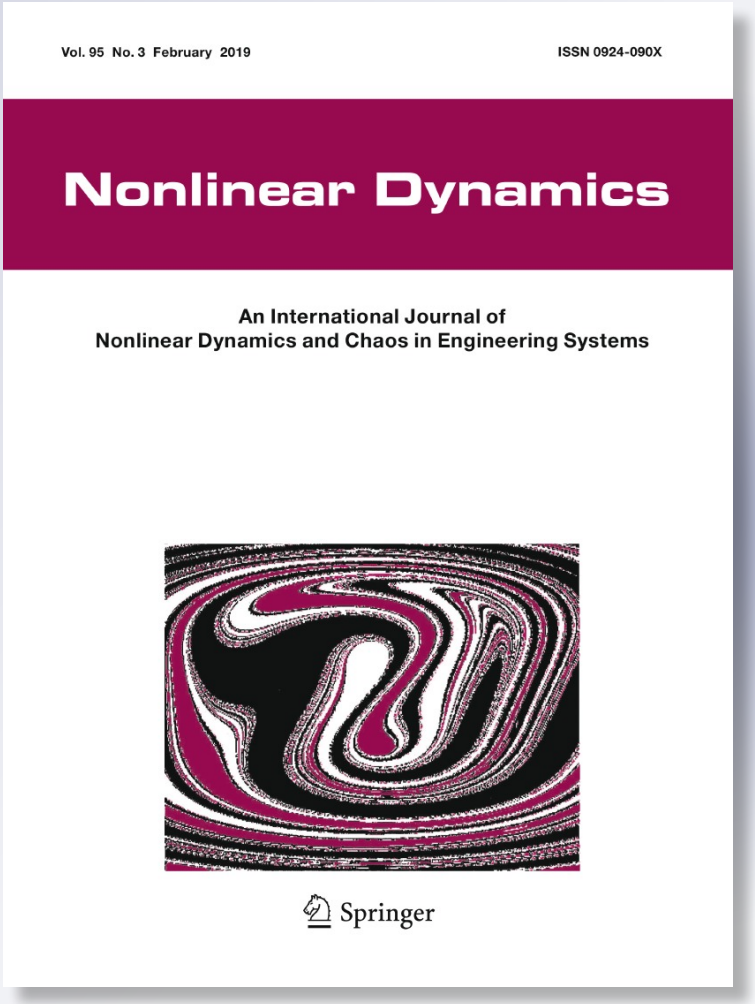

Springer

Nonlinear Dyn (2019) 95:2103–2116
https://doi.org/10.1007/s11071-018-4679-y

ORIGINAL PAPER

Reconstruction of ensembles of nonlinear neurooscillators with sigmoid coupling function

Ilya V. Sysoev · **Vladimir I. Ponomarenko** · **Mikhail D. Prokhorov**

Received: 26 July 2018 / Accepted: 23 November 2018 / Published online: 5 December 2018

Abstract Inferring information about interactions between oscillatory systems from their time series is a highly debated problem. However, many approaches for solving this problem consider either linear systems or linear couplings. We propose a method for the reconstruction of ensembles of nonlinearly coupled neurooscillators described by first-order nonlinear differential equations. The method is based on the minimization of a special target function for each oscillator in the ensemble separately. To find the solution of optimization problem the nonlinear least-squares routine is used. The method does not exploit any parameterization for approximation of nonlinear functions of individual nodes. In addition, an original two-step algorithm for the removal of spurious couplings is proposed based on the clusterization of coefficients of the reconstructed coupling functions and the analysis of their variation. The method efficiency is shown for periodic and chaotic vector time series for ensembles of different size that contain from 8 to 32 oscillators. These oscillators have a cubic nonlinearity and sigmoid is considered as a coupling function. The effect of measurement noise on the results of coupling architecture reconstruction is studied in detail and the method is shown to be effective for relatively high noise (signal to noise ratio equal to eight).

Keywords Network reconstruction · Time series · Neurooscillators · Nonlinear coupling

I. V. Sysoev (✉) · V. I. Ponomarenko
Saratov State University, 83, Astrakhanskaya str., Saratov, Russia 410012
e-mail: ivssci@gmail.com

I. V. Sysoev · V. I. Ponomarenko · M. D. Prokhorov
Saratov Branch of the Institute of Radioengineering and Electronics of Russian Academy of Sciences, 38, Zelyonaya str., Saratov, Russia 410019

1 Introduction

A complex dynamics may originate from very simple systems, if they are coupled in a large network. There are a lot of different examples of such a behavior [1]. The neural network models are of the particular interest, since many neurological processes, both normal and pathological ones are considered to be a network phenomena [2]. One of the simplest models of neural network (1) has been proposed by Sompolinsky et al. [3]:

$$\dot{x}_i = -x_i + \sum_{j=1, j\neq i}^{D} h_{i,j}(g x_j),$$
$$h_{i,j}(x) = k_{i,j} \tanh(x), \qquad (1)$$

where $i = 1, \ldots, D$, D is the number of neurooscillators in the network, $h_{i,j}$ is a coupling function characterizing the influence $j \to i$, i. e., from the jth neurooscillator to the ith one, g is a scaling factor, and $k_{i,j}$ is a coupling coefficient characterizing the strength of coupling $j \to i$. It was analytically proven that in the limit $D \to \infty$ the network elements exhibit a chaotic

behavior [3]. It was also shown numerically that networks composed of sufficiently large number of neurooscillators (about 1000 nodes) can also demonstrate a chaotic dynamics [3].

An approach to the reconstruction of the model (1) from its chaotic vector time series has been proposed recently [4]. This approach and other similar methods [5–9] can be applied for the detection of couplings between the network elements in climate science [10], neuroscience [11], cardiology [12], and some other fields along with the widespread methods like Granger causality [13,14], partial directed coherence [15], directed transfer function [16], phase modeling techniques [17–20], and other similar techniques [21,22], including techniques specially developed for weak coupling [23,24]. Some of recently proposed methods even offer possibility of analysis online [25,26]. A new approach to the problem of model reconstruction was proposed recently [27–30]. This approach considers all dynamical variables to be measured, but nonlinear functions are unknown. Additionally, it is assumed that these functions can be well approximated by a few of well known elementary functions like polynomials (see [31]), sinusoids, logarithms and so on. Therefore, the matrix of many different approximations is fitted, but this matrix is considered to be sparse. However, authors state [27] that the method does not scale well for large systems (an ensemble is considered as a single large system) due to very fast growth of complexity with the increase in number of equations.

Many methods for inferring the interaction topology of networks usually have a number of limitations such as an assumption of weak couplings between the nodes, the need to know the structure of model equations, the absence of noise, etc. [32–36]. For example, our recent method [4] was developed for networks composed of linear oscillators, which perform chaotic oscillations in the absence of noise.

In the present paper, we extend our method [4] to a more general situation. Instead of the linear oscillators, we consider the case where the intrinsic dynamics of network nodes is described by a nonlinear equation. Moreover, we consider now a more general type of the coupling function, which is assumed to be a sigmoid. Limitation to the class of sigmoid functions is essential for the systems under study providing the ability for parameterization in a special way of Richards' curve [37] with a small number of parameters. The proposed method is based on the minimization of a special target function for each oscillator in the ensemble. Since the parameterization of Richards' curve is nonlinear, we use the nonlinear least-squares routines, namely the Levenberg–Marquardt [38,39] algorithm and Trust Region Reflective algorithm [40] for solving the optimization problem instead of the usually used linear least-squares method.

As a result of the method application, we obtain the recovered coefficients of bidirectional coupling between each pair of oscillators in the ensemble. However, in a typical case, the oscillators in the ensemble are not coupled all-to-all and some of the recovered coupling coefficients are redundant. We propose an original two-step algorithm for the removal of spurious couplings based on the clusterization of coefficients of the reconstructed coupling functions and the analysis of their variation. This algorithm allows one to reconstruct the coupling architecture. The specific of reconstruction for sparse networks was recently mentioned [28]. Therefore, removal of spurious couplings can help in better reconstruction of nonlinear functions of individual nodes and coupling functions.

Another distinction of our method from the method [4] is its efficiency not only for chaotic time series, but also for periodic and quasiperiodic regimes and transient processes. We study the dependence of the accuracy of our method on the length of time series and the size of ensemble. The robustness of the proposed approach to measurement noise is also considered. The importance of testing reconstruction algorithms in the presence of measurement noise has been pointed in a number of recent works [9,41,42].

2 Method

We consider the following generalization of the original model (1):

$$\dot{x}_i(t) = f_i(x_i(t)) + \sum_{j=1, j\neq i}^{D} h_{i,j}(g_j(x_j(t) - x_{j,0})), \quad (2)$$

where $f_i(x)$ is an arbitrary continuous function (nonlinear in the general case), $h_{i,j}(x)$ is an arbitrary sigmoid coupling function, $x_{j,0}$ is a shift parameter, and g_j is an amplitude parameter.

2.1 Target function

Assume that we have a vector time series $\{\mathbf{x}(t_n)\}_{n=1}^{N}$ of oscillations in all nodes of the ensemble (2) recorded with a constant sampling time $\Delta t = t_{n+1} - t_n$, where $\mathbf{x}(t_n) = \big(x_1(t_n), x_2(t_n), \ldots, x_D(t_n)\big)$, n is the time index, and N is the total number of samples for each oscillator. For simplicity, let us denote $x_i(t_n) = x_i(n)$. Then, for $(m-1)/2 < n < N-(m-1)/2$ we find numerically the time derivatives $\dot{x}_i(n)$ using the Savitzky–Golay filter [43], where m is a number of points used for smoothing. The filter is useful for reducing the impact of high-frequency noises that are always present in the experimental time series. So, we can rewrite (2) in the following form:

$$f_i(x_i(n)) = \dot{x}_i(n) - \sum_{j=1, j\neq i}^{D} h_{i,j}(g_j(x_j(n) - x_{j,0})). \quad (3)$$

Following the recently proposed approaches [4,6], for each oscillator, we sort the values of $x_i(n)$ in ascending order and denote this sorting as transformation Q_i, which assigns a point with the index $Q_i(n)$ in the sorted time series to a point with the index n in the original time series. We denote the inverse transformation as Q_i^{-1}, which assigns a point with the index n in the original time series to a point with the index $Q_i(n)$ in the sorted time series. Thus, we have $n = Q_i^{-1}(Q_i(n))$. If some point has the index n in the original time series and the index $Q_i(n)$ in the sorted time series, then the neighbor point to the left of this point in the sorted time series has the index $Q_i(n) - 1$. The index of this neighbor point in the original time series is $p_i(n) = Q_i^{-1}(Q_i(n) - 1)$. The points with the indices $Q_i(n)$ and $Q_i(n) - 1$ in the sorted time series are neighbors and the values x_i in these points are close under the assumption that f_i is a continuous function. Consequently, the values of the dynamical variable in the points with the indices n and $p_i(n)$ in the original time series are also close and the function values $f_i\big(x_i(n)\big)$ and $f_i\big(x_i(p_i(n))\big)$ must be close. We denote the difference between these function values as $\delta_i(n)$.

$$\delta_i(n) = f_i(x_i(n)) - f_i(x_i(p_i(n))) = \Delta\dot{x}_i(n) - \sum_{j=1, j\neq i}^{D} \Delta h_{i,j}(n),$$

$$\Delta\dot{x}_i(n) = \dot{x}_i(n) - \dot{x}_i(p_i(n)),$$

$$\Delta h_{i,j}(n) = h_{i,j}(x_j(n)) - h_{i,j}(x_j(p_i(n))). \quad (4)$$

If $N \to \infty$, all $\delta_i(n)$ approach zero under the assumption of the finite variance of x_i. However, if the oscillation regime is rather complex, then the close values of $x_i(n)$ and $x_i(p_i(n))$ does not necessarily imply the proximity of $\dot{x}_i(n)$ and $\dot{x}_i(p_i(n))$. Hence, the right-hand side of Eq. (4) can tend to zero for $N \to \infty$ only as a sum of all its terms. Let us assume that sigmoid coupling function $h_{i,j}$ depends on the parameters $\mathbf{c}_i$. Then, these parameters $\mathbf{c}_i$ must be set in a proper way to provide the convergence to zero of the right-hand side of Eq. (4) with the increase in the number of samples N.

Thus, given a time series of sufficiently large length N, the sum of squares of all $\delta_i(n)$ values can be considered as a target function S_i:

$$S_i(\mathbf{c}_i) = \sum_{n=1, Q_i(n)\neq 1}^{N} \delta_i^2(n), \quad (5)$$

where N is the number of samples. The minimization of (5) allows one to determine all unknown parameters $\mathbf{c}_i$ of coupling function and to define the coupling function $h_{i,j}$ explicitly. Then, the function f_i can be tabulated using, e.g., (3) for all considered n.

2.2 Approximating coupling functions

Let us here consider the task of coupling function approximation in detail. An arbitrary sigmoid function can be satisfactory approximated with a Richards' curve [37]:

$$h_{i,j}(x) = \frac{c_{1,i,j}}{\big(1 + c_{2,i,j}\exp(c_{3,i,j}x)\big)^{c_{4,i,j}}} + c_{5,i,j}. \quad (6)$$

In particular, the hyperbolic tangent is a special case of Eq. (6), while arctangent and error function can be approximated by Eq. (6) with a good accuracy, but not exactly.

Since the minimization of the target function (5) implies the fitting of many coupling functions simultaneously, in the presence of measurement noise, a certain simplification of Eq. (6) is necessary. Without large loss of generality, we set $c_{4,i,j} = 1$ and $c_{5,i,j} = 0$, and rewrite Eq. (6) as follows:

$$h_{i,j}(x) = \frac{c_{1,i,j}}{\left(1 + c_{2,i,j}\exp(c_{3,i,j}x)\right)}. \quad (7)$$

The first simplification reduces the approximating power of the algorithm a little bit, but it helps much in convergence, since it removes a parameter of power in denominator. The second simplification is forced by the fact that Eq. (2) contains a sum of coupling functions, and therefore, there is no need to have many independent constants. Therefore, the original driving term introduced in [3]) is a special case of sum of (7) if one takes into account that the constant can be included into the nonlinear function f_i.

To be able to apply the numerical minimization algorithms, all unknown coefficients must be rewritten in the form of a single vector. Since the reconstruction is performed independently for each ith neurooscillator, it is possible to have a matrix of unknown coefficients, composed of columns, corresponding to different oscillators. Thus, let us rewrite the 3D array $c_{k,i,j}$ in the form of matrix as follows:

$$c_{i,3j+k} = c_{k,i,j}, \quad k = 1, 2, 3. \quad (8)$$

Using (8) the formula (7) can be rewritten in the following form:

$$h_{i,j}(x) = \frac{c_{i,3j+1}}{\left(1 + c_{i,3j+2}\exp(c_{i,3j+3}x)\right)}. \quad (9)$$

2.3 Target function optimization

The target function (5) depends on the parameters $c_{i,3j+2}$ and $c_{i,3j+3}$ nonlinearly, when the coupling functions are approximated as (9). Therefore, using linear least-squares routine as in some previous studies [4,7] is not possible. The nonlinear optimization techniques first demand some reasonable starting guesses for all parameters $\mathbf{c}_i$ (this can be done from a priori knowledge or just arbitrary) and second demand to provide some way to calculate the Jacobi matrix $\mathfrak{J}$ for the target function S.

While the Jacobi matrix $\mathfrak{J}$ always can be approximated by finite differences, this implies additional computational errors, demands to provide a reasonable step in the parameter space and increases calculation time. For the considered case, $\mathfrak{J}$ can be written analytically. Let us differentiate the coupling function (9) for $c_{i,3j+1}$, $c_{i,3j+2}$, and $c_{i,3j+3}$ separately:

$$\frac{\partial h_{i,j}(x)}{\partial c_{i,3j+1}} = \frac{1}{\left(1 + c_{i,3j+2}\exp(c_{i,3j+3}x)\right)} = h'_{i,j}(c_{3j+1}, n), \quad (10)$$

$$\frac{\partial h_{i,j}(x)}{\partial c_{i,3j+2}} = -\frac{c_{i,3j+1}\exp(c_{i,3j+3}x)}{\left(1 + c_{i,3j+2}\exp(c_{i,3j+3}x)\right)^2} = h'_{i,j}(c_{3j+2}, n), \quad (11)$$

$$\frac{\partial h_{i,j}(x)}{\partial c_{i,3j+3}} = -\frac{c_{i,3j+1}c_{i,3j+2}x\exp(c_{i,3j+3}x)}{\left(1 + c_{i,3j+2}\exp(c_{i,3j+3}x)\right)^2} = h'_{i,j}(c_{3j+3}, n). \quad (12)$$

The Jacobi matrix consists of $(N-\theta_i-1)\times 3(D-1)$ elements. Its element with indices n and l can be written in the following form:

$$\mathfrak{J}_{n,l} = h'_{i,j}(c_l, n) - h'_{i,j}(c_l, p_i(n)). \quad (13)$$

Further, the numerically highly efficient `MINPACK` [44] realization of the Levenberg–Marquardt algorithm [38,39] was mostly used for the nonlinear least-squares. If this approach failed to converge, the Trust Region Reflective algorithm [40] realized in popular `Pyhton` numerical library `scipy.optimize` [45] was used.

2.4 Removal of spurious couplings

In a typical case, a node in an ensemble is not connected to all other nodes and some couplings are missing. Therefore, after the model (2) reconstruction, some coupling functions can be superfluous. These functions make a small contribution to the target function. Since the amplitude of coupling function $h_{i,j}$ is determined mostly by the parameter $c_{i,3j+1}$, the K-nearest neighbors approach was used to split the couplings into two clusters, namely the cluster of actual couplings and the cluster of spurious couplings. Analogously to the previously proposed technique for time-delayed feedback oscillators [6], clusterization was performed based on values of $z_{i,j}$ which are the logarithms of absolute values of each of $D(D-1)$ coefficients $c_{i,3j+1}$ $\forall i, j = 1, \ldots N, i \neq j$ in the ensemble:

$$z_{i,j} = \ln(|c_{i,3j+1}|). \quad (14)$$

To start the K-nearest processing, the initial guesses for means were chosen as the maximum and the minimum

values of $z_{i,j}$ for the cluster of actual and spurious couplings, respectively. Since the task is one-dimensional, the choice of a way to determine a distance is not important, because all known ways in one-dimensional case come to the absolute value of the difference.

After clusterization, the superfluous coupling functions were removed from the model (2), and reconstruction was performed once again. Let us denote the new estimates of coupling function coefficients $\mathbf{c}_i$, obtained after the removal of superfluous functions, as $c'_{i,3j+r}$, $r = 1, 2, 3$ (for this reduced set, some (i, j) pairs corresponding to excluded functions are not allowed) and the original estimates as $c_{i,3j+r}$.

However, the numerical experiment has shown that a lot of spurious couplings still stay in the model in most cases, while there are only very few erroneously removed couplings. To correct this, the second step of removal was proposed. The idea of this step is to compute some relative variance measure of all coupling coefficients for the current coupling function $h_{i,j}$, using, for example, the following formula:

$$\Delta\bar{c}_{i,j} = \sum_{r=1}^{3} \left| \frac{(c_{i,3j+r} - c'_{i,3j+r})}{c_{i,3j+r}} \right|. \tag{15}$$

If the coupling function $h_{i,j}$ is not spurious, then it reflects some actual coupling mechanism, and therefore, the corresponding variance measure $\Delta\bar{c}_{i,j}$ should be small. However, for spurious couplings $\Delta\bar{c}_{i,j}$ should be high, since existing of these coefficients is mostly determined by noise and the method imperfectness, and therefore these coefficients have to be essentially different for different coupling architectures. The threshold value of $\Delta\bar{c}_{i,j} = 0.25$ was used to distinguish between the coefficients to be kept and to be removed. After this second removal, the model reconstruction was performed once again, resulting in new estimates, denoted further as $c''_{i,3j+r}$.

For the second reconstruction (after the K-nearest neighbors removal), the estimates $c_{i,3j+r}$ obtained after the first reconstruction (complete ensemble with all possible couplings) were used as initial guesses. For the third reconstruction, the estimates obtained at the second step, i. e., $c'_{i,3j+r}$ were used as initial guesses. Such an approach reduced the time of reconstruction significantly and improved the convergence of nonlinear least-squares routines.

3 Results

Cubic parabolas were used as functions f_i (16). Coupling functions were chosen as hyperbolic tangent like in the original Eq. (1), but with variant scale parameter g_j and variant shift parameter $x_{0,i}$ as it was proposed in (2):

$$f_i(x) = -\gamma_i x + \alpha_i x^3, \tag{16}$$

$$h_{i,j}(x) = k_{i,j} \tanh(g_j(x - x_{0,i})). \tag{17}$$

Following the original study [3], the values of coupling coefficients $k_{i,j}$ were generated from the normal distribution with a zero mean and the standard deviation equal to $J/\sqrt{D}$, where $J = 6$ was mostly used. Then, some couplings were randomly set to zero. The values of the parameters $x_{i,0}$, γ_i, g_i and α_i were generated from the uniform distributions in the ranges $[-1; 1]$, $[0.5; 1.5]$, $[0.5; 1.5]$, and $[0; 1]$, respectively.

All equations were solved numerically with the fourth-order adaptive Runge-Kutta algorithm, using ODE solver `odeint` included in `scipy.integrate` package [45], with the sampling interval $\Delta t = 0.01$.

The ensembles of $D = 8, 12, 16, 20, 24$, and 32 neurooscillators were considered. In the original study [3], the ensemble of 1000 neurooscillators was considered and chaotic behavior was detected. In the recent paper [4], the ensembles of sufficiently smaller size (from $D = 16$ to $D = 64$) were found be able to produce chaotic oscillations. Here, due to the use of nonlinear functions f_i instead of the linear ones, we revealed the chaotic behavior even for 8 oscillators in the case of 35 nonzero couplings, but this behavior occurred very seldom. In the case of 16 oscillators, the quasiperiodic behavior was also detected.

All regimes were detected after a long transient process of 2^{17} sampling intervals, i. e., about 1300 units of dimensionless time. The periodic regimes were detected using a rule that for the chosen oscillator number i, all values from some parts of time series repeated themselves at least twice with a precision 10^{-6}. To distinguish between quasiperiodic and chaotic regimes the largest Lyapunov exponent λ_1 for the whole ensemble was estimated on the interval of 4000 units of dimensionless time using the algorithm described in [46]. For chaotic regimes, the typical values of λ_1 estimates lied in the range $[0.12; 0.22]$. The regular regimes were characterized by $\lambda_1 \in [-0.05; 0.06]$, assuming that nonzero values appeared due to the finite length of

time series and other algorithm imperfections. Since the ranges corresponding to the chaotic and periodic regimes did not overlap, we considered this technique to be robust enough for detecting the type of the regime.

Usually, one half or 5/8 of possible couplings were kept nonzero in the current study. For the ensembles with small number of nodes ($D \leq 16$), the further reduction of the number of nonzero couplings caused some oscillators to be excluded from the network, and the total network complexity occurred to be not enough to produce chaotic or complex regular oscillations, or even to establish long enough transient process.

The starting guesses for parameters $c_{i,3j+1}$, $c_{i,3j+2}$, and $c_{i,3j+3}$ were set as 0, 1, and 2, respectively. Such a choice corresponds to the not scaled and not shifted hyperbolic tangent.

3.1 Reconstruction of small ensembles in periodic and chaotic regimes

First, let us consider small ensembles of $D = 8$ neurooscillators, since they are more suitable for illustration of results of the method application, and focus on the most typical regimes (periodic and chaotic ones), described also in [3] for original Eq. (1). Figure 1 shows the times series for all oscillators in the ensemble for the cases of periodic regime (Fig. 1a) and chaotic regime (Fig. 1b) in the absence of measurement noise.

The results of nonlinear functions f_i reconstruction for all eight nodes in the presence of additive measurement noise with standard deviation $\sigma_{noise} = 0.05$ are plotted in Fig. 1c for the periodic regime and in Fig. 1d for the chaotic regime. The standard deviation of noise was in the range 1.6%–5.3% for the chaotic regime and in the range 1.9%–5.1% for the periodic regime, depending on the amplitude of oscillations for a particular neurooscillator.

One can see that the reconstruction is successful even for a complex periodic regime. The Savitzky–Golay filter based on averaging over $m = 13$ points and $m = 17$ points was used to improve the estimates of derivatives for the chaotic regime and the periodic regime, respectively. In few cases, the removal of superfluous couplings can help in better nonlinear function reconstruction (see results of f_2 reconstruction for the periodic regime in Fig. 1c).

The quality of reconstruction of coupling architecture depends on the noise level and the oscillation regime. Since all oscillators in the ensemble have to be reconstructed in order to detect the coupling architecture, the possibility to reconstruct the entire ensemble completely is mostly determined by one or some oscillators with the minimal signal to noise ratio.

Figure 2 shows the results of coupling architecture reconstruction for both the periodic (upper row) and the chaotic (lower row) regimes for ensembles of eight neurooscillators. The indicated noise levels correspond to the oscillator with the minimal signal to noise ratio. The reconstruction can be successful, even in the presence of high-level noise, especially for a chaotic regime. In this particular case, the time series consisting of $N = 2^{14}$ points (Fig. 1a, b) were used.

It should be noted that using longer time series mostly results in reduction of the number of errors in the coupling architecture recovery for chaotic regimes, since new additional information about network dynamics is provided. For instance, for the case considered in Fig. 2, the missing coupling from the sixth to the fourth oscillator in the chaotic regime can be detected correctly if the length of time series is increased in eight times or more. To characterize the dependence of results of reconstruction on the time series length we also introduced the mean error of reconstruction of the coupling coefficients $k_{i,j}$. If the actual coupling function is hyperbolic tangent, it can be estimated as $-2c_{i,3j+1}$ using the approximation (9). So, the mean relative error for coupling magnitude reconstruction can be calculated as follows:

$$\langle \Delta \tilde{k}_{i,j} \rangle = \sum_{i=1}^{D} \sum_{j=1, j\neq i}^{D} \left| \frac{k_{i,j} + 2c''_{i,3j+1}}{k_{i,j}} \right|, \quad \text{if } k_{i,j} \neq 0 \text{ and } c_{i,3j+1} \neq 0. \tag{18}$$

Note that this mean error does not reflect the errors in coupling architecture reconstruction. The dependence of $\langle \Delta \tilde{k}_{i,j} \rangle$ on the length of time series for three different noise levels is shown in Fig. 3 for the same ensembles as considered above.

The dependence $\langle \Delta \tilde{k}_{i,j} \rangle(N)$ is flat for the noise level equal to 1%. For the larger noise levels, the results more depend on the guesses for initial conditions, and finding a global minimum becomes a challenge, especially for a chaotic regime. The same problem was previously mentioned for another reconstruction technique [47], for which the use of very long time series was shown to be inefficient due to the existence of many local minima of the target function. This problem can be partly addressed using some special fraction techniques [48].

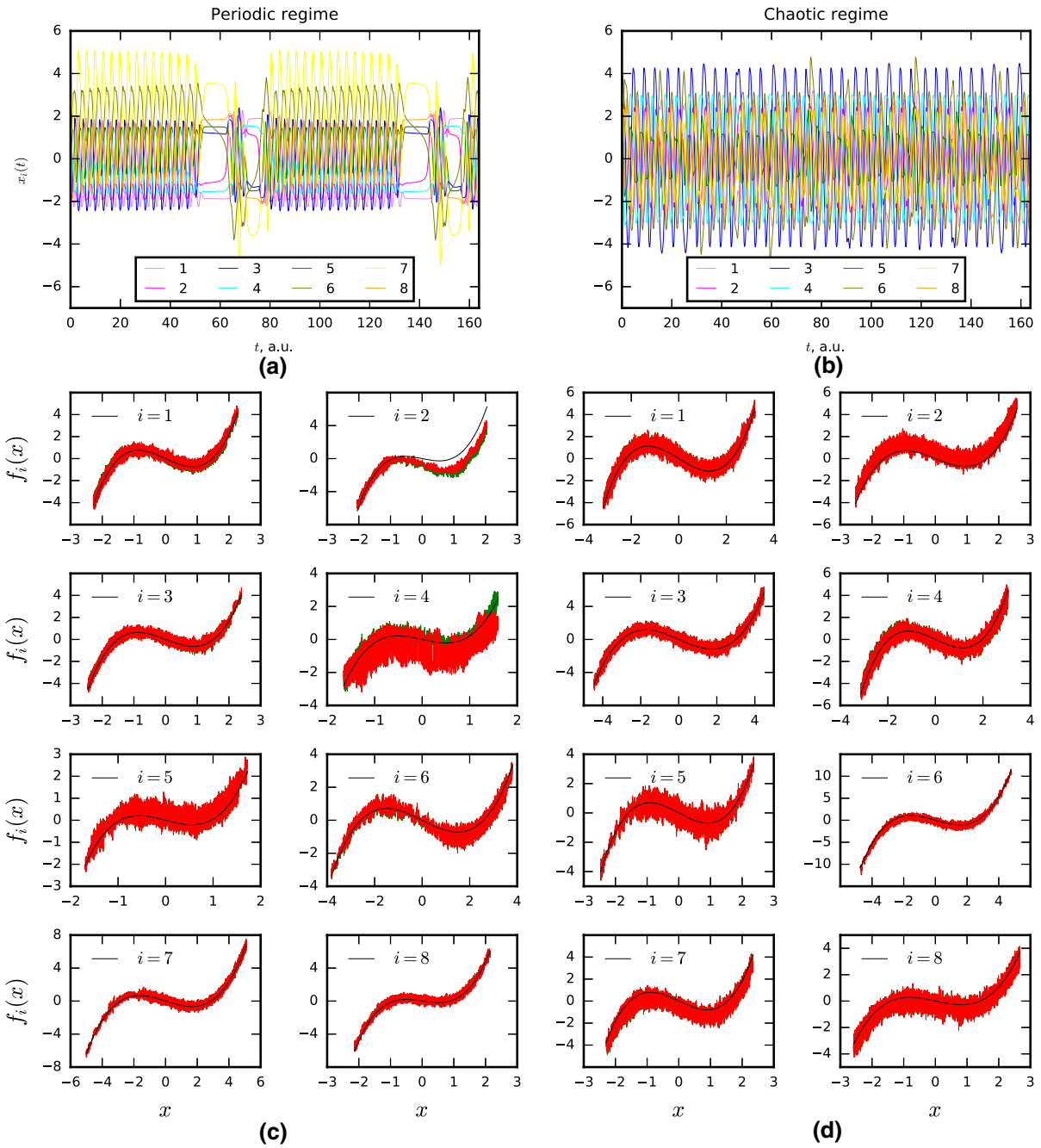

Fig. 1 Time series of the ensemble (2) of $D = 8$ neurooscillators with 35 nonzero couplings (5/8 of the maximal possible number) in the periodic regime (**a**), and in the chaotic regime (**b**), for which the reconstruction was successful. Reconstructed coupling functions of all 8 neurooscillators for the periodic regime (**c**) and for the chaotic regime (**d**); original functions are shown in black and the functions reconstructed in the presence of measurement noise are shown in green (before removal of spurious couplings) and in red (after removal). (Color figure online)

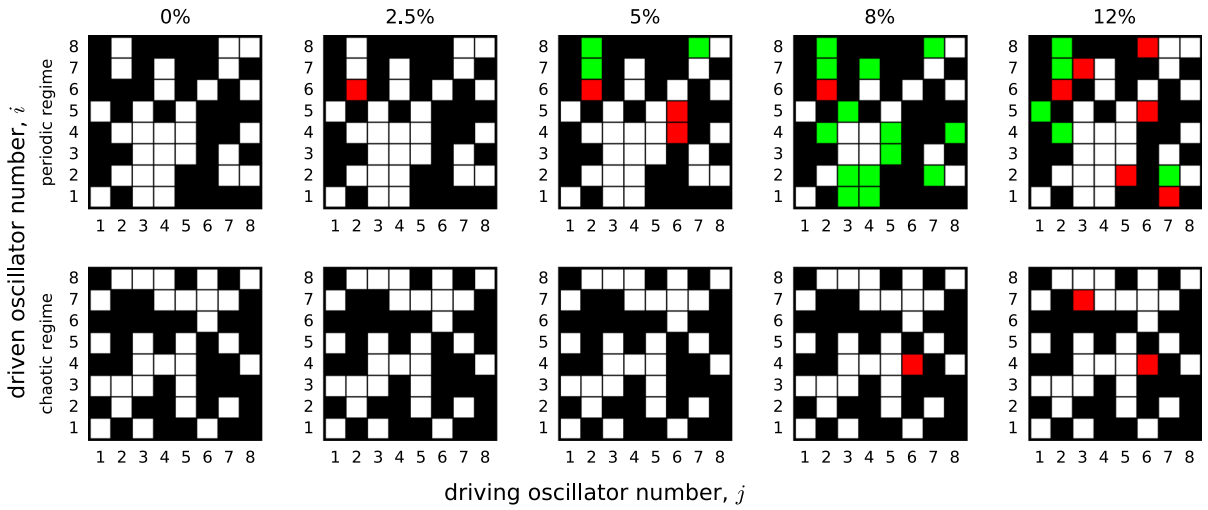

Fig. 2 Schemes of coupling architecture reconstruction for the periodic (upper row) and the chaotic (lower row) regimes for ensembles of $D = 8$ neurooscillators for different noise levels indicated in percent. The numbers of driving neurooscillators are shown on the horizontal axis, while the numbers of driven oscillators are shown on the vertical axis. Detected existing couplings (black), removed from the model nonexisting couplings (white), spuriously detected couplings (green), and missed existing couplings (red) are plotted by squares. (Color figure online)

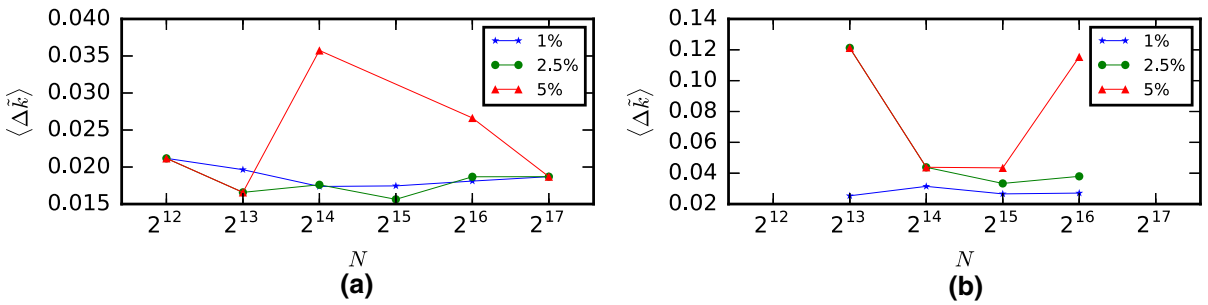

Fig. 3 Dependence of the mean error in the coupling coefficient reconstruction (18) on the length of time series N for the periodic regime (**a**) and for the chaotic regime (**b**) for three noise levels: 1%, 2.5%, and 5% with respect to the signal standard deviation

To estimate the efficiency of the reconstruction procedure, 100 different ensembles with nonequilibrium behavior were simulated. Only four from these 100 ensembles demonstrated a chaotic dynamics. For all of these four ensembles, the reconstruction was successful, including the reconstruction in the presence of additive 2–12% measurement noise (e. g., see Fig. 2). The reconstruction was also successful for two complex periodic regimes. One of them is shown in Fig. 1a. For most of other periodic regimes, the reconstruction of equations was successful only for part of nodes. The main reason for this is that some oscillators demonstrated too simple dynamics. Usually, successful reconstruction in periodic regime was possible, when each period included at least eight or ten oscillations (we consider one oscillation to be a part of series between two local minima or maxima in the absence of measurement noise).

Figure 4 depicts all coupling functions reconstructed in the presence of 5% measurement noise for the chaotic ensemble, which time series are plotted in Fig. 1b. One can see that most functions are reconstructed with a good accuracy. Sometimes, the functions obtained after removal of spurious couplings occur to be closer to the original ones (for instance, see $h_{7,3}$ and $h_{4,6}$) than the same functions reconstructed before the removal. For periodic regimes, the results of

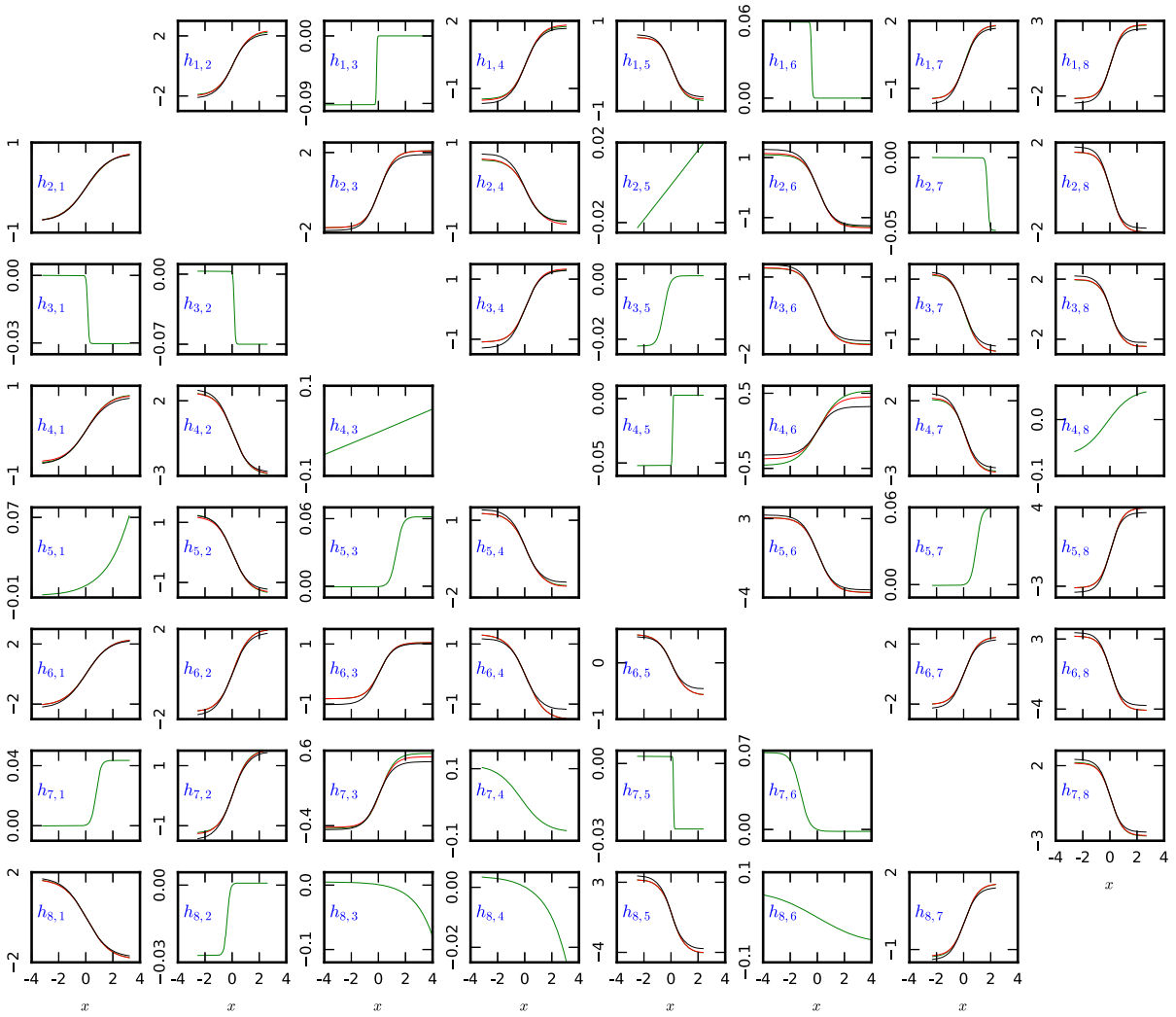

Fig. 4 Original (black), reconstructed (green), and reconstructed after removal of spurious couplings (red) coupling functions $h_{i,j}$ for the ensemble of 8 nodes in the chaotic regime, which time series are plotted in Fig. 1b. In most cases, all these three lines: black, green, and red are overlapping because of accurate reconstruction. (Color figure online)

the coupling function reconstruction are usually similar to those presented in Fig. 4 for the chaotic regime.

3.2 Reconstruction of large ensembles for periodic and chaotic regimes and for long transient process

Consideration of larger networks with more than 8 nodes is important due to two reasons: first, the method scalability is demonstrated, second, the larger networks can produce greater number of different regimes. In the current study, we focused on the long transient processes in addition to chaotic and periodic regimes, since transient processes are of great importance in many practical applications, especially in biology. We detected transients by considering very long time series, at the end of which a fixed point or simple periodic solution was found. Then, only a part of this realization having the same length as the considered chaotic and regular regimes was used for the ensemble reconstruction. We also kept in mind that some very long transients could behave as chaotic regimes. Therefore, for chaotic regimes we examined the Lyapunov exponents twice using the first and the second half of

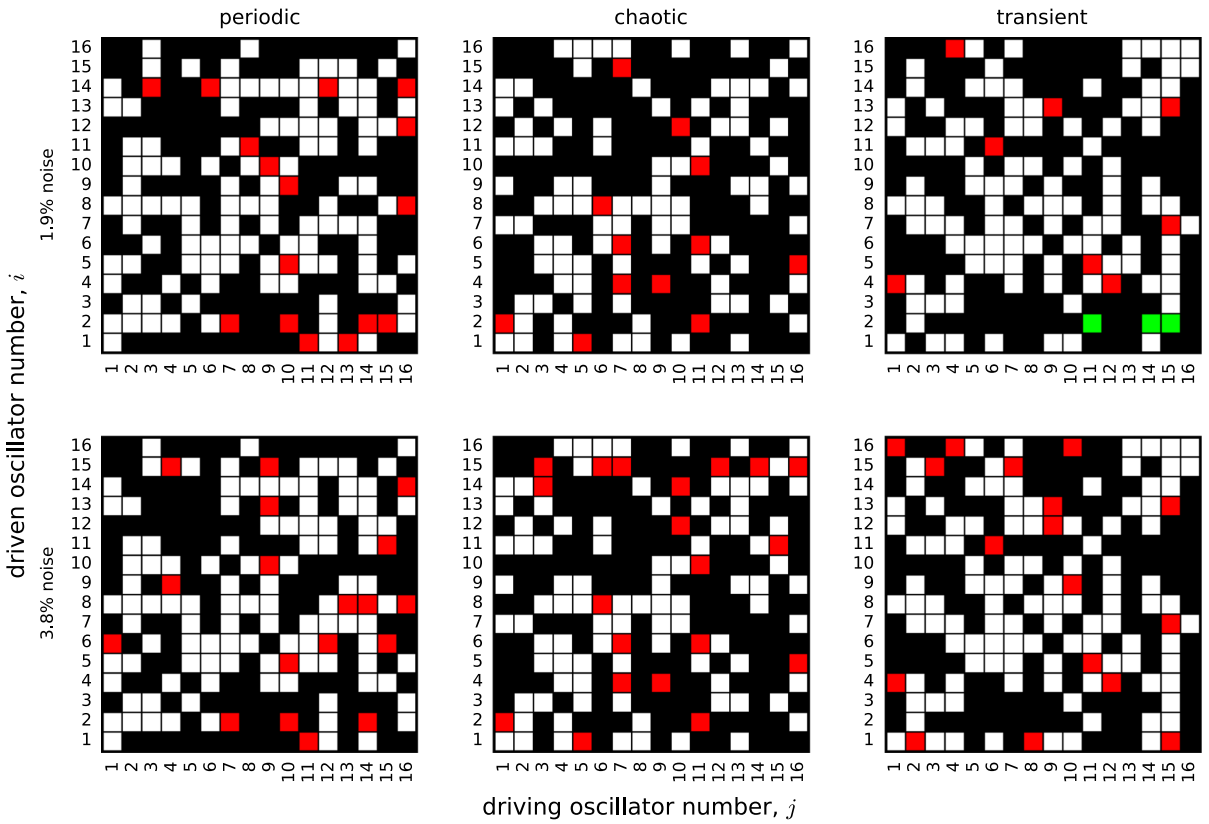

Fig. 5 Schemes of coupling architecture reconstruction for the periodic regime (left column), chaotic regime (center column), and transient process (right column) for ensembles of $D = 16$ neurooscillators for two different levels of noise indicated in percent. The numbers of driving oscillators are shown on the horizontal axis, while the numbers of driven oscillators are shown on the vertical axis. Detected existing couplings (black), removed from the model nonexisting couplings (white), spuriously detected couplings (green), and missed existing couplings (red) are plotted by squares. (Color figure online)

the time series separately. If the Lyapunov exponent decreased significantly in the second half of the time series, it could be the sign of nonstationarity and could be the marker of possible transient. As a result of this approach application, we excluded one chaotic regime and classified it as a transient process.

In this subsection, we consider the reconstruction of ensembles with the number of nodes from 12 to 32 for the cases of different noise levels. The series of the same length ($N = 2^{14}$) as for the case of 8 neurooscillators were considered. Generally, the maximal noise level, for which the reconstruction of the whole ensemble can be successful, occurs to be less for larger number of nodes. For 16 nodes, the noise level of 3.6%–4% occurs to be critical.

The results of coupling architecture reconstruction for the three considered regimes are plotted in Fig. 5 for two different levels of noise. It can be seen that the number of missed existing couplings is greater for $D = 16$ than for $D = 8$. It is explained by two main reasons. First, the number of couplings for $D = 16$ is greater than for $D = 8$ at the same length of time series. The second reason is partial synchronization of some nodes in the ensemble at $D = 16$, which makes it impossible to distinguish between some candidates for driving nodes. The presence of both factors makes it hard to find some weak couplings.

Note that smoothing significantly contributes to results of the coupling reconstruction, i. e., varying m one can increase or decrease the number of false posi-

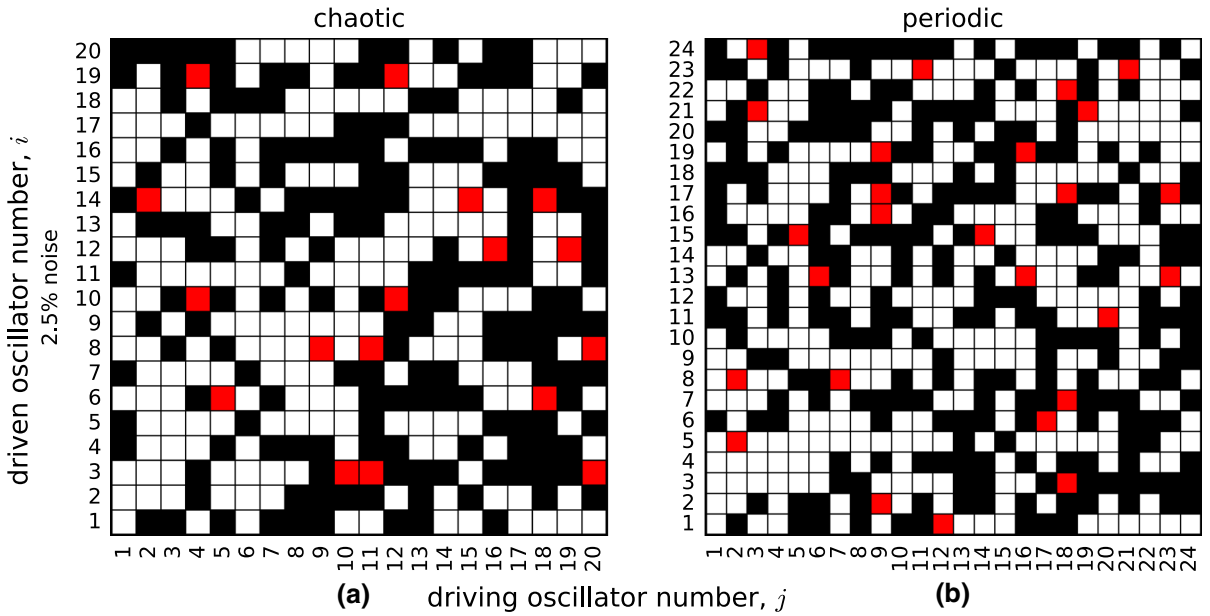

Fig. 6 Schemes of coupling architecture reconstruction for an ensemble of 20 nodes in the chaotic regime (**a**), and for an ensemble of 24 nodes in the periodic regime (**b**). The numbers of driving oscillators are shown on the horizontal axis, while the numbers of driven oscillators are shown on the vertical axis. Detected existing couplings (black), removed from the model nonexisting couplings (white), and missed existing couplings (red) are plotted by squares. (Color figure online)

tives in 1.5–2 times. Usually, better results correspond to larger smoothing, but very high smoothing disturbs the signal shape and, therefore, leads to problems with convergence.

In addition to the cases of $D = 8$ and $D = 16$, we performed successful reconstruction for ensembles of 12, 20, 24, and 32 neurooscillators in chaotic and periodic regimes. For $D = 12$, we found one transient process, which evolved to a periodic regime in contrast to a transient process, which evolved to a stable fixed point for $D = 16$. The results for 20 oscillators in the chaotic regime and for 24 oscillators in a periodic regime for 2.5% relative measurement noise are shown in Fig. 6. The number of errors in the coupling architecture reconstruction (only missed couplings, no spurious ones) is less than 10% in both cases: 17 errors for 190 actual couplings for $D = 20$ and 26 errors for 276 actual couplings for $D = 24$. In the absence of noise, there were no errors in the coupling architecture reconstruction for both ensembles considered in Fig. 6. We obtained a qualitatively similar result for the ensemble consisting of 32 oscillators. However, the scheme of the coupling architecture reconstruction is very large in this case, and we do not present it.

4 Discussion

A number of specialized approaches were proposed recently for the reconstruction of ensembles of coupled neurooscillators of different nature from their time series [4–7]. Since the inverse problem is generally ill-defined, these techniques intensively use a priori knowledge about the motion equations for individual nodes and coupling functions [41,49]. Being developed for model neurooscillators, they aim applications to real data as ultimate goal. While some electronic system equations were already successfully reconstructed [6] from experimental data, the application of the method to objects of another nature, such as neuroscience and climatology, is still not straightforward. We can mention the three main problems:

1. the individual node equations are too simple and do not match the specifics of experimental systems;
2. the coupling organization, including type of coupling functions is practically unknown;
3. the measurement noise is significant in real applications, but its effects are not tested well.

In the current research, we focused on developing and improving the approach recently proposed [4] for the first-order neurooscillators [3] in order to increase its practical value. We addressed all three mentioned problems:

1. the approach was tuned to deal with nonlinear functions instead of the linear function in the autonomous part of equations;
2. the parameters of nonlinear sigmoid coupling functions were considered to be unknown and reconstructed from data;
3. the effects of measurement noise were studied in detail.

We showed the possibility to reconstruct the network of 8 neurooscillators from their time series containing 2^{12}–2^{14} time points and 10–40 oscillations in the presence of sufficiently high level of noise (up to 12%). This result can be compared to the task of processing records from the real neuroscience intracranial animal experiment [50], where eight brain areas were recorded with the frequency of 2048 Hz and digitized by 16-bit ADC with noise occupying lower 4–5 bits, and then analyzed in the moving window of 0.5–2 s length. Our task is even closer to the task of studying the coupling in stationary physiological states like sleep or epilepsies, which average length is greater (e. g., about 6 s for the absence epilepsy [51]).

The possibility to reconstruct larger networks of 16 and even 32 neurooscillators is of potential interest for human studies, including magnetoencephalography data analysis, or experiments using novel techniques [52], which allow more electrodes to be implemented.

While many researchers prefer to escape applying nonlinear least-squares routine, since it may not converge and its results can depend on initial guesses for coefficients, we show here the successful application of this routine in the case of relatively large number of coefficients (up to 168 in the case of $D = 8$ and up to 720 in the case of $D = 16$, i. e., 364–768 data points per one coefficient), 2/3 of which enter equations nonlinearly in the presence of noise, and for not very long time series (from 2^{14} to 2^{16} points). Possibly, the efficiency of least-squares algorithms can be partly explained by the fact that sigmoid functions are bounded and simple.

The ability of the proposed approach to operate efficiently with recordings from periodic regimes and transient processes is also very important for further practical applications since such types of activity are considered as very common in neuroscience. Though applications to real data demand additional technology tuning and optimization, especially choosing better equations for individual nodes, we believe that obtained progress is significant and promising.

Acknowledgements This research was funded by the Russian Science Foundation, Grant No. 14-12-00291.

Compliance with ethical standards

Conflicts of interest The authors declare that they have no conflict of interest.

References

1. Boccaletti, S., Latora, V., Morenod, Y., Chavez, M., Hwang, D.-U.: Complex networks: structure and dynamics. Phys. Rep. **424**, 175–308 (2006)
2. Sporns, O., Chialvo, D.R., Kaiser, M., Hilgetag, C.C.: Organization, development and function of complex brain networks. Trends Cognit. Sci. **8**(9), 418–425 (2004)
3. Sompolinsky, H., Crisanti, A., Sommers, H.E.: Chaos in random neural networks. Phys. Rev. Lett. **61**(3), 259–262 (1988)
4. Sysoev, I.V., Ponomarenko, V.I., Pikovsky, A.: Reconstruction of coupling architecture of neural field networks from vector time series. Commun. Nonlinear Sci. Numer. Simulat. **57**, 342–351 (2018)
5. Shandilya, S.G., Timme, M.: Inferring network topology from complex dynamics. N. J. Phys. **13**(1), 013004 (2011)
6. Sysoev, I.V., Ponomarenko, V.I., Kulminsky, D.D., Prokhorov, M.D.: Recovery of couplings and parameters of elements in networks of time-delay systems from time series. Phys. Rev. E **94**, 052207 (2016)
7. Pikovsky, A.: Reconstruction of a neural network from a time series of firing rates. Phys. Rev. E **93**, 062313 (2016)
8. Xu, Y., Zhou, W., Fang, J.: Topology identification of the modified complex dynamical network with non-delayed and delayed coupling. Nonlinear Dyn. **68**(1–2), 195–205 (2012)
9. Yang, X., Wei, T.: Revealing network topology and dynamical parameters in delay-coupled complex network subjected to random noise. Nonlinear Dyn. **82**, 319–332 (2015)
10. Mokhov, I.I., Smirnov, D.A.: El Niño – southern oscillation drives north atlantic oscillation as revealed with nonlinear techniques from climatic indices. Geophys. Res. Lett. **33**, L03708 (2006)
11. Kaminski, M., Brzezicka, A., Kaminski, J., Blinowska, K.: Measures of coupling between neural populations based on Granger causality principle. Front. Comput. Neurosci. **10**(OCT), 114 (2016)
12. Porta, A., Faes, L.: Wiener–Granger causality in network physiology with applications to cardiovascular control and neuroscience. Proceedings of the IEEE, **12** (2015)
13. Chen, Y., Rangarajan, G., Feng, J., Ding, M.: Analyzing multiple nonlinear time series with extended Granger causality. Phys. Lett. A **324**(1), 26–35 (2004)

14. Kornilov, M.V., Medvedeva, T.M., Bezruchko, B.P., Sysoev, I.V.: Choosing the optimal model parameters for Granger causality in application to time series with main timescale. Chaos, Solitons Fractal. **82**, 11–21 (2016)
15. Baccala, L., Sameshima, K.: Partial directed coherence: a new concept in neural structure determination. Biol. Cybern. **84**, 463–474 (2001)
16. Kamiński, M., Ding, M., Truccolo, W.A., Bressler, S.L.: Evaluating causal relations in neural systems: Granger causality, directed transfer function and statistical assessment of significance. Biol. Cybern. **85**, 145–157 (2001)
17. Rosenblum, M.G., Pikovsky, A.S.: Detecting direction of coupling in interacting oscillators. Phys. Rev. E **64**, 045202(R) (2001)
18. Tokuda, I.T., Jain, S., Kiss, I.Z., Hudson, J.L.: Inferring phase equations from multivariate time series. Phys. Rev. Lett. **99**, 064101 (2007)
19. Koutlis, C., Kugiumtzis, D.: Discrimination of coupling structures using causality networks from multivariate time series. Chaos **26**, 093120 (2016)
20. Kralemann, B., Pikovsky, A., Rosenblum, M.: Reconstructing phase dynamics of oscillator networks. Chaos **21**, 025104 (2011)
21. Wu, X., Wang, W., Zheng, W.X.: Inferring topologies of complex networks with hidden variables. Phys. Rev. E **86**, 046106 (2012)
22. Yang, G., Wang, L., Wang, X.: Reconstruction of complex directional networks with group lasso nonlinear conditional Granger causality. Sci. Rep. **7**(1), 2991 (2017)
23. Smirnov, D.A., Andrzejak, R.G.: Detection of weak directional coupling: phase-dynamics approach versus state-space approach. Phys. Rev. E **71**, 036207 (2005)
24. De Feo, O., Carmeli, C.: Estimating interdependences in networks of weakly coupled deterministic systems. Phys. Rev. E **77**(2), 026711 (2008)
25. Wu, X., Sun, Z., Liang, F., Yu, C.: Online estimation of unknown delays and parameters in uncertain time delayed dynamical complex networks via adaptive observer. Nonlinear Dyn. **73**(3), 1753–1768 (2013)
26. Shemyakin, V., Haario, H.: Online identification of large-scale chaotic system. Nonlinear Dyn. **93**(2), 961–975 (2018)
27. Wang, W., Yang, R., Lai, Y., Kovanis, V., Grebogi, C.: Predicting catastrophes in nonlinear dynamical systems by compressive sensing. Phys. Rev. Lett. **106**, 154101 (2011)
28. Han, X., Shen, Z., Wang, W.-X., Di, Z.: Robust reconstruction of complex networks from sparse data. Phys. Rev. Lett. **114**, 28701 (2015)
29. Brunton, S., Proctor, J., Kutz, J.: Discovering governing equations from data by sparse identification of nonlinear dynamical systems. Proc. Natl. Acad. Sci. U. S. A. **113**, 3932–7 (2016)
30. Mangan, N., Brunton, S., Proctor, J., Kutz, J.: Inferring biological networks by sparse identification of nonlinear dynamics. IEEE Trans. Mol. Biol. Multi-Scale Commun. **2**, 52–63 (2016)
31. Casadiego, J., Nitzan, M., Hallerberg, S., Timme, M.: Model-free inference of direct network interactions from nonlinear collective dynamics. Nat. Commun. **8**, 2192 (2017)
32. Gouesbet, G., Meunier-Guttin-Cluzel, G., Menard, O.: Chaos and its Reconstruction. Nova Science Publishers, New York (2003)
33. Bezruchko, B.P., Smirnov, Da: Extracting Knowledge From Time Series: (An Introduction to Nonlinear Empirical Modeling). Springer Series in Synergetics. Springer, New York (2010)
34. Wang, W.-X., Lai, Y.-C., Grebogi, C.: Data based identification and prediction of nonlinear and complex dynamical systems. Phys. Rep. **644**, 1–76 (2016)
35. Timme, M., Casadiego, J.: Revealing networks from dynamics: an introduction. J. Phys. A Math. Theor. **47**, 343001 (2014)
36. Smirnov, D.A.: Quantifying causal couplings via dynamical effects: a unifying perspective. Phys. Rev. E **90**, 062921 (2014)
37. Richards, F.J.: A flexible growth function for empirical use. J. Exp. Bot. **10**(2), 290–300 (1959)
38. Levenberg, K.: A method for the solution of certain nonlinear problems in least squares. Q. Appl. Math. **2**, 164–168 (1944)
39. Marquardt, D.: An algorithm for least-squares estimation of nonlinear parameters. SIAM J. Appl. Math. **11**(2), 431–441 (1963)
40. Coleman, T.F., Li, Y.: An interior trust region approach for nonlinear minimization subject to bounds. SIAM J. Opt. **6**, 418–445 (1996)
41. Kera, H., Hasegawa, Y.: Noise-tolerant algebraic method for reconstruction of nonlinear dynamical systems. Nonlinear Dyn. **85**(1), 675–692 (2016)
42. Upadhyay, R.K., Mondal, A., Paul, C.: A method for estimation of parameters in a neural model with noisy measurements. Nonlinear Dyn. **85**(4), 2521–2533 (2016)
43. Savitzky, A., Golay, M.: Smoothing and differentiation of data by simplified least squares procedures. Anal. Chem. **38**(8), 1627–1639 (1964)
44. Moré, J.J., Sorensen, D.C., Hillstrom, K.E., Garbow, B.S.: The minpack project. In: Cowell, W.J. (ed.) Sources and Development of Mathematical Software, pp. 88–111. Prentice-Hall, Upper Saddle River (1984)
45. Millman, K.J., Aivazis, M.: Python for scientists and engineers. Comput. Sci. Eng. **13**, 9–12 (2011)
46. Rosenstein, M.T., Collins, J.J., De Luca, C.J.: A practical method for calculating largest Lyapunov exponents from small data sets. Physica D: Nonlinear Phenom. **65**, 117–134 (1993)
47. Baake, E., Baake, M., Bock, H., Briggs, K.: Fitting ordinary differential equations to chaotic data. Phys. Rev. A **45**(8), 5524–5529 (1992)
48. Sysoev, I.V., Smirnov, D.A., Bezruchko, B.P.: Identification of chaotic systems with hidden variables (modified Bock's algorithm). Chaos, Solitons Fractal. **29**, 82–90 (2006)
49. Smirnov, D.A., Sysoev, I.V., Seleznev, E.P., Bezruchko, B.P.: Global reconstruction from nonstationary data. Tech. Phys. Lett. **29**(10), 824–827 (2003)
50. Lüttjohann, A., van Luijtelaar, G.: The dynamics of cortico-thalamo-cortical interactions at the transition from pre-ictal to ictal lfps in absence epilepsy. Neurobiol. Dis. **47**, 47–60 (2012)

51. Coenen, A.M.L., van Luijtelaar, E.L.J.M.: Genetic animal models for absence epilepsy: a review of the WAG/Rij strain of rats. Behav. Genet. **33**, 635–655 (2003)
52. Jun, J.J., Steinmetz, N.A., Siegle, J.H., Denman, D.J., Bauza, M., Barbarits, B., Lee, A.K., Anastassiou, C.A., Çağatay Aydın, A.A., Barbic, M., Blanche, T.J., Bonin, V., Couto, J., Dutta, B., Gratiy, S.L., Gutnisky, D.A., Häusser, M., Karsh, B., Ledochowitsch, P., Lopez, C.M., Mitelut, C., Musa, S., Okun, M., Pachitariu, M., Putzeys, J., Rich, P.D., Rossant, C., lung Sun, W., Svoboda, K., Carandini, M., Harris, K.D., Koch, C., O'Keefe, J., Harris, T.D.: Fully integrated silicon probes for high-density recording of neural activity. Nature **551**, 232–236 (2017)